



Research article

Telaprevir is a potential drug for repurposing against SARS-CoV-2: computational and *in vitro* studies

Amal Mahmoud^{a,**}, Ahmed Mostafa^{b,*}, Ahmed A. Al-Karmalawy^c, Ahmad Zidan^{d,e},
Hamada S. Abulkhair^{c,f}, Sara H. Mahmoud^b, Mahmoud Shehata^b, Mahmoud M. Elhefnawi^g,
Mohamed A. Ali^b

^a Department of Biology, College of Science, Imam Abdulrahman Bin Faisal University, P.O. Box. 1982, 31441, Dammam, Saudi Arabia

^b Center of Scientific Excellence for Influenza Viruses, National Research Centre, 12622 Dokki, Giza, Egypt

^c Department of Pharmaceutical Chemistry, Faculty of Pharmacy, Horus University-Egypt, New Damietta 34518, Egypt

^d Department of Bioinformatics, Genetic Engineering and Biotechnology Research Institute (GEBRI), University of Sadat City, Egypt

^e Clinical Research Team, Monof Chest Hospital, Ministry of Health, Egypt

^f Department of Pharmaceutical Organic Chemistry, Faculty of Pharmacy, Al-Azhar University, Nasr City 11884, Cairo, Egypt

^g Biomedical Informatics and Cheminformatics Group, Informatics and Systems Department, National Research Centre, Cairo, Egypt

ARTICLE INFO

Keywords:

Anti-HCV
Drug repurposing
Telaprevir
Protease inhibitor
SARS-CoV-2

ABSTRACT

Drug repurposing is an important approach to the assignment of already approved drugs for new indications. This technique bypasses some steps in the traditional drug approval system, which saves time and lives in the case of pandemics. Direct acting antivirals (DAAs) have repeatedly repurposed from treating one virus to another. In this study, 16 FDA-approved hepatitis C virus (HCV) DAA drugs were studied to explore their activities against severe acute respiratory syndrome coronavirus 2 (SARS-CoV-2) human and viral targets. Among the 16 HCV DAA drugs, telaprevir has shown the best *in silico* evidence to work on both indirect human targets (cathepsin L [CTSL] and human angiotensin-converting enzyme 2 [hACE2] receptor) and direct viral targets (main protease [M^{PRO}]). Moreover, the docked poses of telaprevir inside both hACE2 and M^{PRO} were subjected to additional molecular dynamics simulations monitored by calculating the binding free energy using MM-GBSA. *In vitro* analysis of telaprevir showed inhibition of SARS-CoV-2 replication in cell culture (IC₅₀ = 11.552 μM, CC₅₀ = 60.865 μM, and selectivity index = 5.27). Accordingly, based on the *in silico* studies and supported by the presented *in vitro* analysis, we suggest that telaprevir may be considered for therapeutic development against SARS-CoV-2.

1. Introduction

The coronavirus disease 2019 (COVID-19) pandemic caused by severe acute respiratory syndrome corona virus 2 (SARS-CoV-2) infection has created devastating impacts on social, economic, political, and health aspects, with still no satisfactory therapy currently approved [1].

Coronaviruses are generally positive-sense single-stranded RNA pathogens belonging to the Coronaviridae family. Structurally, the virus includes four essential proteins, including a helical nucleocapsid formed of nucleocapsid (N), membrane (M), envelope (E), and club-shaped spike (S) proteins [2]. The major part (two-thirds of the viral genome) of the coronavirus genome is the ORF1a/b gene. ORF1a/b codes for 16 nonstructural proteins (nsp1-16) using viral-encoded proteases [3].

Coronaviruses have caused three severe respiratory outbreaks so far: severe acute respiratory syndrome coronavirus (SARS-CoV) in 2002/2003, Middle East respiratory syndrome coronavirus (MERS-CoV) in 2012, and SARS COV-2 in 2019 [4, 5]. The SARS-CoV-2 pandemic is a great challenge for all humankind that needs to be addressed quickly and properly. Drug repurposing is a good technique for the rapid discovery of a medication in emergency cases such as the COVID-19 pandemic [6, 7, 8].

Low-risk and low-cost drug repurposing approaches have been widely applied to identify new therapeutic indications for commercially available drugs or old drugs, especially during pandemics or fatal epidemics. The main advantage of drug repurposing in drug development is that it spares the time, cost, and efforts that are exerted in the research and

* Corresponding author.

** Corresponding author.

E-mail addresses: amhsalem@iau.edu.sa (A. Mahmoud), ahmed_elsayed@daad-alumni.de (A. Mostafa).

development process [6, 9, 10, 11]. Interestingly, drug repurposing or repositioning strategies have been intensively applied during the COVID-19 pandemic, and a large-scale drug repositioning survey for SARS-CoV-2 antivirals has so far been achieved [6, 12, 13]. For instance, eight out of the 12 FDA-approved antivirals from 2012 to 2017 were HCV antivirals repurposed to treat other viruses (e.g., Zika and Ebola viruses) [14, 15]. HCV direct-acting antivirals (DAAs) are predicted to target some coronavirus-related elements, including indirect human targets (e.g., angiotensin converting enzyme 2 [ACE2] and cathepsin L [CTSL]) or direct viral targets (e.g., S protein and main protease [M^{Pro}]) [16, 17, 18, 19, 20].

The ACE2 receptor plays two crucial roles in SARS-CoV-2 infection and its pathophysiology. First, it is important for viral entry into infected host cells by binding to the protease-activated receptor-binding domain (RBD) of the invading virus spike (S) protein, initiating a new viral

replication/infection cycle. Second, it plays a significant role in organ damage alleviation via its effect on the renin-angiotensin-aldosterone system (RAAS) [21, 22].

CTSL plays an important role in the viral infection and replication cycle. It facilitates proteolysis of the S1 subunit of the viral S protein, which enables the binding of the viral S protein to the host cell ACE2 receptor. Following virus entry by endocytosis, CTSL contributes to the fusion process and the release of viral genetic material into the host cell [23].

The spike (S) protein of SARS-CoV-2 interacts with the human ACE2 (hACE2) receptor to gain entry into the host cell to initiate infection. The SARS-CoV-2 S protein is cleaved into S1 and S2 subunits, with S1 serving the function of receptor-binding and immunogenic domains and S2 serving the function of membrane fusion. The antigenic drift in S protein through accumulation of mutations can drastically affect the SARS-CoV-2

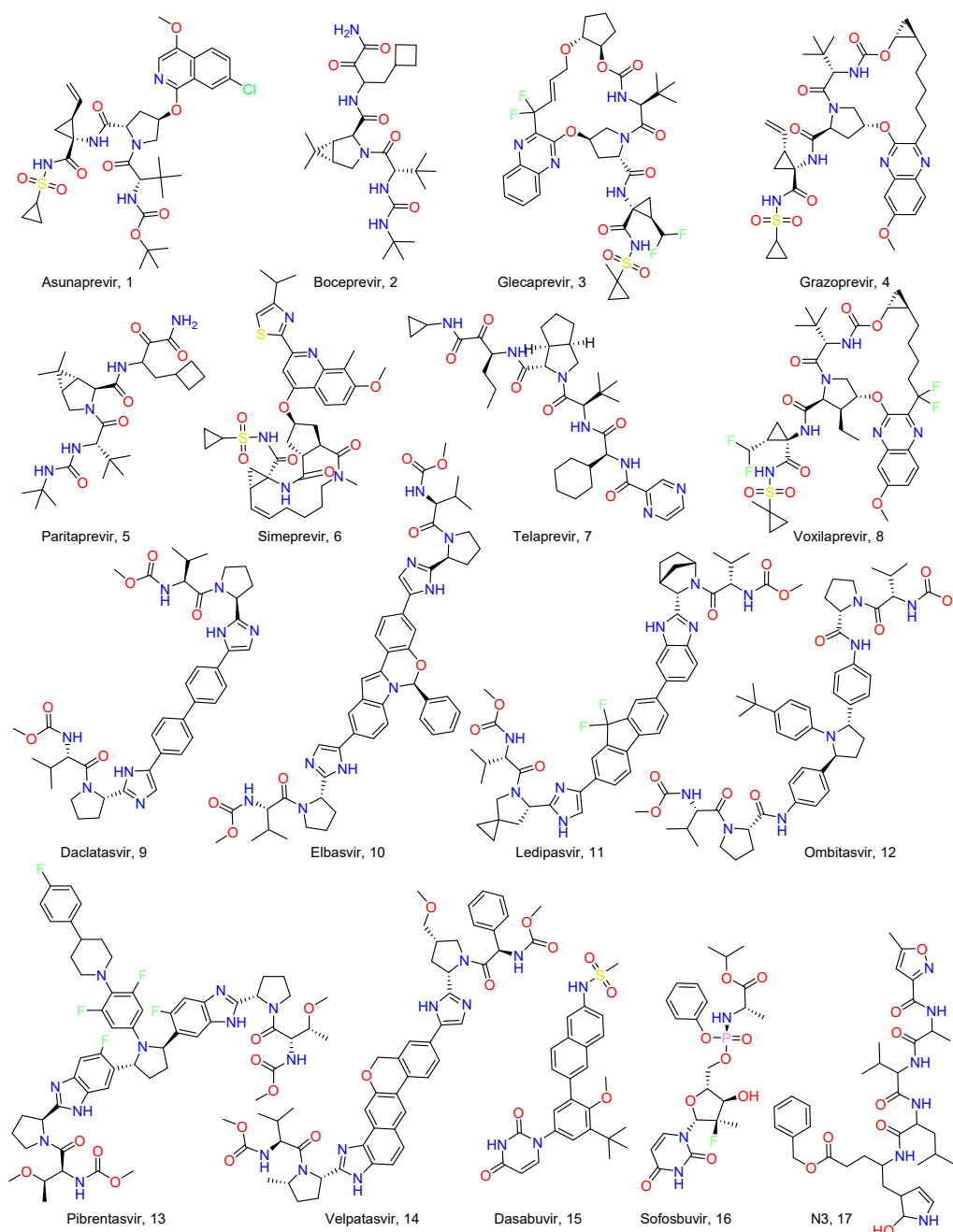


Figure 1. Chemical structures of direct acting anti-hepatitis C virus drugs (HCV DAAs) and N3 inhibitor.

phenotype, including replication efficiency, antigenic properties, and pathogenicity [24].

M^{Pro} resides in nsp5 and is a key protein with proteolytic activity as the main protease. This protein is highly conserved among coronaviruses and plays an important role in mediating viral replication and transcription machinery, making it an attractive and highly specific drug target for SARS-CoV-2 [20, 25, 26], with little or no impact on cellular proteases [17].

Importantly, the extensive use of currently approved FDA-approved drugs under the “Emergency Use Authorization (EUA)” with the huge global distribution of SARS-CoV-2 virus prompted the evolution of several mutants which may be accompanied with decreased binding affinity and drug-resistance [27]. To this point, more studies are required to promote other FDA-approved drugs as new anti-SARS-CoV-2 drugs, especially in the case of drug-resistant variants [28, 29]. In this study, we aimed to investigate the drug repurposing of 16 FDA-approved HCV DAA (listed in Figure 1) against SARS-CoV-2 via indirect targeting of hACE2 and CTSL, and direct targeting of S and M^{Pro}. This was achieved using in silico approaches and validated with an in vitro experiment for the most promising drug candidates.

2. Results and discussion

2.1. In silico analysis

2.1.1. Similarity ensemble approach

Among the selected HCV DAAs (Figure 1), three drugs (elbasvir [DB11574], boceprevir [DB08873], and telaprevir [DB05521]) were predicted to act on two highly relevant targets for SARS-CoV-2 (hACE2 and CTSL). The results are summarized in Table 1.

The in vitro activity of both boceprevir and telaprevir against CTSL was retrieved using a poly pharmacology browser, as previously reported in the literature [30]. hACE2 was retrieved using the SEA server tool as a significant target for Elbasvir. As mentioned previously, hACE2 is a highly relevant drug target for SARS-CoV-2. The CTSL was retrieved for both boceprevir and telaprevir using the SEA server with highly significant P-values. Both SwissTarget Prediction and PPB retrieved CTSL as a target for boceprevir and telaprevir with probability = 1. This means that both boceprevir and telaprevir have already been tested in vitro and have reported activities on CTSL.

2.1.2. Docking studies

First, a validation process was performed for the Molecular Operating Environment (MOE) program by subjecting the SARS-CoV-2 M^{Pro} target to a separate redocking process for only its co-crystallized inhibitor (N3) inside its binding pocket (Figure 2), and a low RMSD value indicated a valid performance (RMSD = 1.43) [31, 32]. It can be noted that the docked N3 inhibitor (represented in green color) is superimposed on the native co-crystallized one (represented in red colour) forming one H-bond with Met45 and one pi-H bond with Thr26 amino acids. On the other hand, the native co-crystallized N3 inhibitor is characterized by its covalent bond with Cys145 amino acid. Moreover, it formed six H-bonds

with Thr190, Glu166, Gln189, His164, and Gly143 amino acids, besides one H-pi interaction with His41 amino acid as well.

Molecular docking of asunaprevir (1), boceprevir (2), glecaprevir (3), grazoprevir (4), paritaprevir (5), simeprevir (6), telaprevir (7), voxilaprevir (8), daclatasvir (9), elbasvir (10), ledipasvir (11), ombitasvir (12), pibrentasvir (13), velpatasvir (14), dasabuvir (15), and sofosbuvir (16) into the binding pockets of both hACE2 and M^{Pro} receptors of SARS-CoV-2 were performed including the co-crystallized N3 inhibitor (17) in case of M^{Pro} docking. They stabilized within the previously mentioned binding pockets with promising scores and binding modes with the amino acids of both receptors. The binding scores, in addition to the detailed binding modes of the 16 FDA-approved HCV DAAs with the amino acids of both hACE2 and M^{Pro} pockets, are depicted in Table 2 and Supplementary Figure S1.

Regarding the docking results of the 16 FDA-approved HCV DAA drugs against hACE2 receptor, their descending binding order was found to be: pibrentasvir (13) > telaprevir (7) > elbasvir (10) > ombitasvir (12) > velpatasvir (14) > daclatasvir (9) > ledipasvir (11) > glecaprevir (3) > simeprevir (6) > asunaprevir (1) > voxilaprevir (8) > grazoprevir (4) > paritaprevir (5) > boceprevir (2) > sofosbuvir (16) > dasabuvir (15). This result is not consistent with the previously published molecular simulation study by Kateryna and Anna, who virtually tested and analysed 248 drugs including some HCV DAA drugs “missing Telaprevir” against the receptor-binding domain (RBD) of spike glycoprotein of SARS-CoV-2, and speculated that the HCV drugs ledipasvir and paritaprevir are the most efficient binders to the RBD when used together with a natural biflavonoid amentoflavone [33].

The descending order for their docking against M^{Pro} protein was: telaprevir (7) > glecaprevir (3) > docked co-crystallized n3 inhibitor (17) > grazoprevir (4) > ombitasvir (12) > voxilaprevir (8) > simeprevir (6) > boceprevir (2) > velpatasvir (14) > asunaprevir (1) > elbasvir (10) > paritaprevir (5) > ledipasvir (11) > pibrentasvir (13) > daclatasvir (9) > sofosbuvir (16) > dasabuvir (15).

Based on the remarkable structural similarity between the substrate binding cleft and active site of the SARS-CoV-2 M^{Pro} of HCV and SARS-CoV-2, it is possible that HCV drugs with anti-protease activity might also inhibit SARS-CoV-2 M^{Pro} [34, 35]. Bafna et al. reported that telaprevir could efficiently inhibit SARS-CoV-2 proteolytic activity and bind to its active site [36].

It is worth mentioning that among the aforementioned tested HCV members, telaprevir was found to be the most promising drug to be repurposed against SARS-CoV-2, where it achieved the best binding affinity towards its main protease and the second-best binding affinity for the hACE2 receptor, indicating a highly promising intrinsic activity compared to other members. Moreover, its binding score towards SARS-CoV-2 M^{Pro} (-10.87 kcal/mol) was found to be superior to that of the docked co-crystallized N3 inhibitor (17) of the M^{Pro} (-10.01 kcal/mol) as presented in Table 3.

Telaprevir was found to be stabilized within the hACE2 receptor (including a part of the RBD), which is used by SARS-CoV-2 to enter and initiate COVID-19 infection. It formed three H-bonds with His345, Glu402, and Glu375 amino acids at 2.93, 2.99, and 3.58 Å, respectively. In addition, it is obvious that it bound the Zn²⁺ ion of the hACE2 through

Table 1. Prediction of HCV DAAs against SARS-CoV-2.

No.	Drug name	Tool used	Score of prediction	Retrieved target	Relevance score from gene cards
1	Elbasvir	SEA server	P-value = 6.319e-06	Human angiotensin converting enzyme II (hACE2)	59.95
2	Boceprevir	SwissTargetPrediction	Probability = 1	Cathepsin L (CTSL)	15.47
		SEA server	P-value = 0.009643		
		PPB	Probability = 1		
3	Telaprevir	SwissTargetPrediction	Probability = 1		
		SEA server	P-value = 1.511e-12		
		PPB	Probability = 1		

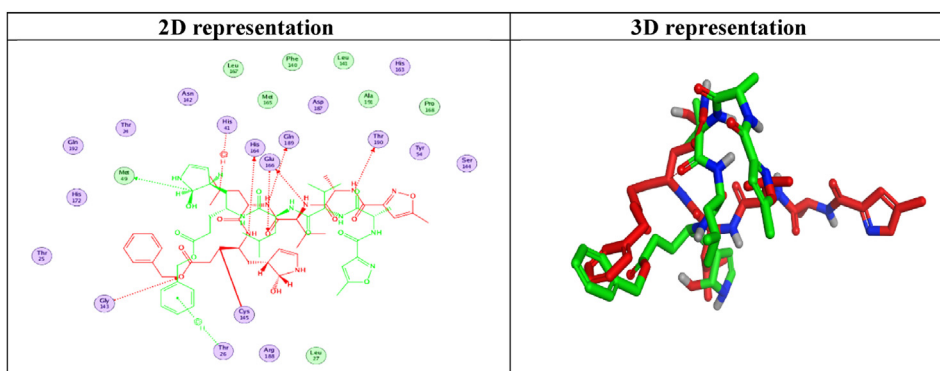


Figure 2. 2 D and 3 D representations showing the re-docking process between the native co-crystallized inhibitor (N3) (represented in red) and the docked one (represented in green) at M^{Pro} pocket.

Glu375 amino acid bridge, which indicates an extra promising inhibitory activity. In addition, it fitted very well inside the hACE2 receptor, as depicted in Table 3. However, telaprevir interactions with the M^{Pro} pocket of SARS-CoV-2 were observed to be through the formation of three H-bonds with Gln189, His164, and Met49 amino acids at 3.39, 3.41, and 3.86 Å, respectively. In addition, it showed a very promising fit inside the M^{Pro} binding site of SARS-CoV-2 (Table 3).

Collectively, telaprevir was predicted to be the most promising member among the 16 tested FDA-approved HCV DAA drugs, to be tested further in vitro in order to confirm its inhibitory activity against SARS-CoV-2.

2.1.3. Molecular dynamics (MD) simulations

In order to gain a deeper insight into the stability of telaprevir (7) in the binding pockets of both the hACE2 and M^{Pro} pockets of SARS-CoV-2 in two separate runs, MD simulations [37] were performed for a simulation time of 100 ns. Moreover, the co-crystallized N3 inhibitor of M^{Pro} was subjected to a separate run as a reference standard.

Analyses of both the root mean square deviation (RMSD) and root mean square fluctuation (RMSF) for the three docked poses of telaprevir (hACE2), telaprevir (M^{Pro}), and N3 (M^{Pro}), respectively, are depicted in Figure 3.

The RMSD (left Y-axis) is an important quantitative measurement for evaluating the stability of the protein structure throughout the simulation period. The protein RMSD trajectory for the docked telaprevir in hACE2 receptor pocket showed a fluctuation till reaching 10 ns simulation time, gradually showed equilibrium till reaching 64 ns fluctuating within the range of 1.0 Å, and then returned again to an equilibrium state within a fluctuation range of 0.9 Å (Figure 3A). In contrast, the protein RMSD for the docked telaprevir in M^{Pro} pocket showed a stability manner till reaching 20 ns fluctuating within the range of 1.1 Å, then fluctuated within range of 0.6 Å till reaching 60 ns, and finally fluctuated within the range of 1.0 Å till the end of the simulation time (Figure 3B). Furthermore, the docked N3 in the M^{Pro} pocket fluctuated up to 10 ns and then fluctuated within the range of 1.0 Å until the end of the simulation time (Figure 3C).

RMSF is useful for monitoring local changes within the protein chain during simulation. It was obvious that the binding site amino acids showed the lowest local conformational changes with telaprevir (< 2.5 Å) compared to the reference standard in the case of M^{Pro}. This finding confirmed the conformational stability of the binding pocket during the simulation. In addition, both tails (N- and C- terminal regions) showed higher RMSF values, which matches with the expected high flexibility of their loop structures, unlike other alpha helices and beta sheets, which are usually more rigid.

Ligand RMSD (right Y-axis) indicates the stability of the docked pose with respect to the protein, especially its binding pocket. It is worth mentioning that the docked pose of Telaprevir in the M^{Pro} pocket

(Figure 3B) showed both the lowest RMSD and the lowest fluctuations (within the range of 2.8 Å) during the simulation time compared to its docked pose in the hACE2 pocket (Figure 3A) and the docked pose of the co-crystallized inhibitor (N3) of M^{Pro} as well (Figure 3C), indicating its higher stability inside the M^{Pro} pocket of SARS-CoV-2.

The binding interaction histogram for each protein–ligand complex during the simulation is shown in Figure 4. In the case of the docked pose of telaprevir in the hACE2 pocket of SARS-CoV-2, the amino acids Ser43, Ser47, Tyr50, Asn51, His345, Phe274, Pro346, Ala348, Thr371, Glu375, Tyr510, and Arg518 contributed mainly to the hydrogen bonding interactions (5%–50%), and Phe40, Tyr50, Ile54, Met62, Val343, His345, Pro346, Trp349, His374, His378, Phe504, Tyr510, and Arg514 had the greatest contribution to the hydrophobic interactions (2%–28%) with the docked pose of telaprevir. Ser43, Ser44, Ser47, Tyr50, Tyr51, Met62, Asn63, Trp69, Glu145, Arg273, Val343, Cys344, His345, Pro346, Thr347, Ala348, Cys361, Lys363, Asp367, Asp368, Thr371, His374, Glu375, Glu398, Glu402, Glu406, Ser409, His505, Tyr510, Arg514, Tyr515, and Arg518 contributed mainly to the water bridge hydrogen bonds (1%–27%) with the docked telaprevir (Figure 4A). In contrast, telaprevir formed stronger interactions inside the binding pocket of SARS-CoV-2 M^{Pro} compared to its hACE2 pocket throughout the simulation time, as can be observed from the timeline protein–ligand contacts (Figure 4B). His41, Asn142, Cys145, Glu166, Arg188, Gln189, and Trp190 amino acids contributed to 5%–100% to the hydrogen bonding interactions with telaprevir in the M^{Pro} pocket. However, the amino acids Leu27, Met49, Cys145, Met165, Leu167, and pro168 contributed mainly to the hydrophobic interactions (5%–25%), while Thr24, Ser46, Asn142, Gly143, Glu166, Gln189, and Thr190 showed the highest contribution to the water bridge hydrogen bonds (30%–70%) to the telaprevir pose in the M^{Pro} pocket of SARS-CoV-2. Finally, regarding the docked pose of N3 inside the binding pocket of M^{Pro}, it was found that amino acids Thr26, His41, Asn142, Gly143, Ser144, Cys145, His164, Glu166, Gln189, Thr190, and Gln192 had the largest percentage of hydrogen bonding interactions (10%–70%); the amino acids Met49, Cys145, Met165, Leu167, and Pro168 contributed to the hydrophobic interactions with (5%–20%); and the amino acids Thr24, Thr25, His41, Ser46, Asn119, Leu141, Asn142, Gly143, Ser144, Cys145, His163, His164, Met165, Glu166, Leu167, Pro168, Arg188, Gln189, Thr190, Ala191, and Gln192 contributed to (5%–190%) of the water bridge hydrogen bonding (Figure 4C).

Figure 5 shows the heat map for the total number of contacts and interactions for telaprevir within the hACE2 and M^{Pro} pockets, in addition to the N3 inhibitor inside the M^{Pro} pocket of SARS-CoV-2 protein. It was observed that the main binding site for telaprevir inside the hACE2 pocket was Tyr510 throughout >80% of the simulation time (Figure 5A). In contrast, the main binding residues inside the M^{Pro} pocket were found to be His41, Gln189, and Glu166 throughout the simulation time (80%–99%) (Figure 5B). However, the main binding amino acids for the N3

Table 2. The binding scores and modes of the examined sixteen FDA approved HCV DAAs against both the hACE2 and M^{pro} receptor pockets of SARS-CoV-2 compared to the docked co-crystallized N3 inhibitor (17) in case of the latter one.

No.	HCV Drug	R ^a	S ^b	RMSD ^c	Amino acid interactions	Distance (Å)
1	Asunaprevir	A	-9.25	1.87	His345/H-acceptor Arg514/H-acceptor Trp349/H-pi	3.08 3.10 4.02
		P	-9.34	1.79	Asn142/H-donor Glu166/H-donor	2.94 3.35
2	Boceprevir	A	-8.16	1.64	Arg518/H-acceptor	3.20
		P	-9.41	1.79	Gln189/H-donor Glu166/H-acceptor Gln189/H-donor Cys145/H-donor	3.02 3.13 3.17 3.88
3	Glecaprevir	A	-9.81	1.73	His345/H-acceptor Phe274/H-pi	3.07 4.29
		P	-10.80	1.90	Gly143/H-acceptor His163/H-acceptor Glu166/H-acceptor Met165/H-donor Met49/H-donor	2.96 2.97 3.31 4.11 4.42
4	Grazoprevir	A	-9.15	1.45	Arg518/H-acceptor Thr276/H-acceptor	2.90 3.23
		P	-10.00	1.68	Asn142/H-acceptor Asn142/H-donor Asn142/H-donor Gln189/pi-H Gln189/pi-H	2.94 3.08 3.22 3.90 4.26
5	Paritaprevir	A	-9.13	1.42	His345/H-donor Arg518/pi-H Arg518/pi-H	3.14 3.50 4.67
		P	-9.04	1.91	Glu166/H-acceptor Asn142/pi-H Asn142/pi-H	3.09 4.04 4.24
6	Simeprevir	A	-9.77	1.77	Ala348/H-donor His345/pi-pi	3.73 3.67
		P	-9.39	1.53	His41/H-pi Gly143/pi-H	3.54 3.57
7	Telaprevir	A	-11.86	1.53	His345/H-acceptor Glu402/H-donor Glu375/H-donor	2.93 2.99 3.58
		P	-10.87	1.91	Gln189/H-donor His164/H-donor Met49/H-donor	3.39 3.41 3.86
8	Voxilaprevir	A	-9.19	1.82	Glu375/H-donor Glu402/H-donor Arg514/pi-H Arg514/pi-H Arg514/pi-H	3.42 3.51 3.84 4.09 4.42
		P	-9.57	1.69	Asn142/H-acceptor Glu166/H-acceptor Met49/H-donor	2.84 2.86 3.53
9	Daclatasvir	A	-10.46	1.53	Arg514/pi-H Gln442/H-acceptor Arg514/pi-H	3.27 3.39 3.60
		P	-8.64	1.52	Glu166/H-acceptor Thr26/pi-H	2.96 4.26
10	Elbasvir	A	-11.22	1.97	His374/H-donor His345/pi-H His345/pi-pi Arg518/pi-H	4.27 3.73 3.86 4.14
		P	-9.33	1.70	Thr26/H-acceptor Thr25/H-acceptor Glu166/pi-H Glu166/pi-H	3.13 3.33 4.12 4.23
11	Ledipasvir	A	-10.44	2.13	Arg514/H-acceptor Arg514/H-acceptor Glu406/H-acceptor	3.02 3.03 3.40
		P	-9.04	1.61	Thr24/H-donor Glu166/H-acceptor	3.01 3.31

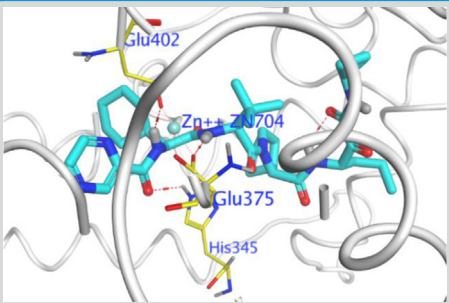
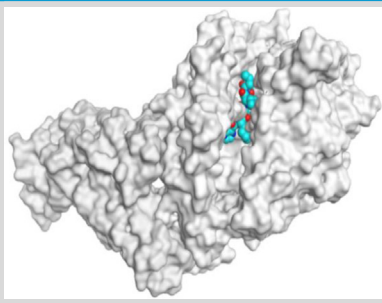
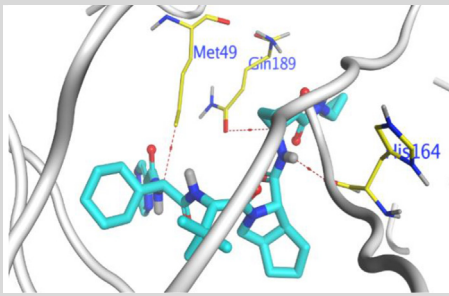
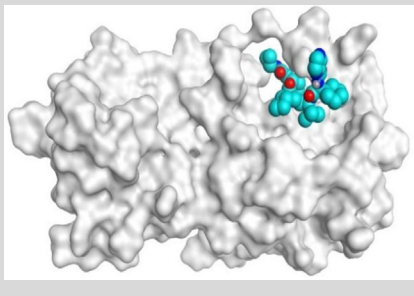
(continued on next page)

Table 2 (continued)

No.	HCV Drug	R ^a	S ^b	RMSD ^c	Amino acid interactions	Distance (Å ^v)
12	Ombitasvir	A	-11.09	2.31	Asp367/H-donor	2.99
		P	-9.61	1.55	Glu166/H-donor	3.18
					Glu166/pi-H	4.74
13	Pibrentasvir	A	-12.39	2.04	His345/H-acceptor	2.93
					Thr276/H-acceptor	3.02
					His345/pi-pi	3.42
					His345/pi-pi	3.53
					Phe504/H-pi	3.57
		P	-8.86	2.17	Thr24/H-acceptor	2.91
14	Velpatasvir	A	-10.85	1.87	Arg518/H-donor	3.24
		P	-9.36	1.54	Ala348/H-donor	3.31
Ala348/H-acceptor	3.32					
Glu406/H-donor	3.35					
Phe274/H-pi	4.45					
Glu166/H-acceptor	3.36					
15	Dasabuvir	A	-7.87	1.47	Gln189/pi-H	4.54
					Glu406/H-donor	3.47
					Glu406/H-donor	3.57
					His345/pi-pi	3.65
		P	-8.03	1.38	Phe504/pi-pi	3.88
					Glu166/H-donor	2.97
16	Sofosbuvir	A	-7.99	1.81	His164/H-donor	3.33
					His41/pi-pi	3.99
					Glu375/H-donor	3.71
		P	-8.41	1.51	His345/pi-pi	3.27
					His378/pi-H	4.30
					His163/H-acceptor	3.18
17	Co-crystallized inhibitor (docked)	P	-10.01		Thr24/H-donor	3.36
					Thr26/H-acceptor	3.44
					Glu166/pi-H	4.41
					Gln189/H-donor	2.88
					Glu166/H-acceptor	3.02
					Thr190/H-donor	3.08

A: hACE2 receptor of SARS-CoV-2.

P: M^{pro} protein of SARS-CoV-2.^a R: The target receptor pocket.^b S: The score of a compound inside the protein-binding pocket (kcal/mol).^c RMSD: The root mean squared deviation between the predicted pose and crystal structure.Table 3. 3D representations showing the binding interactions and protein positioning of the most promising member of the sixteen tested FDA approved HCV drugs (Telaprevir) against both the hACE2 and M^{pro} receptor pockets of SARS-CoV-2.

Drug	R	3D binding interactions	3D pocket positioning
(7)	A		
	P		

Red dash represents H-bonds and black dash represents H-pi interactions.

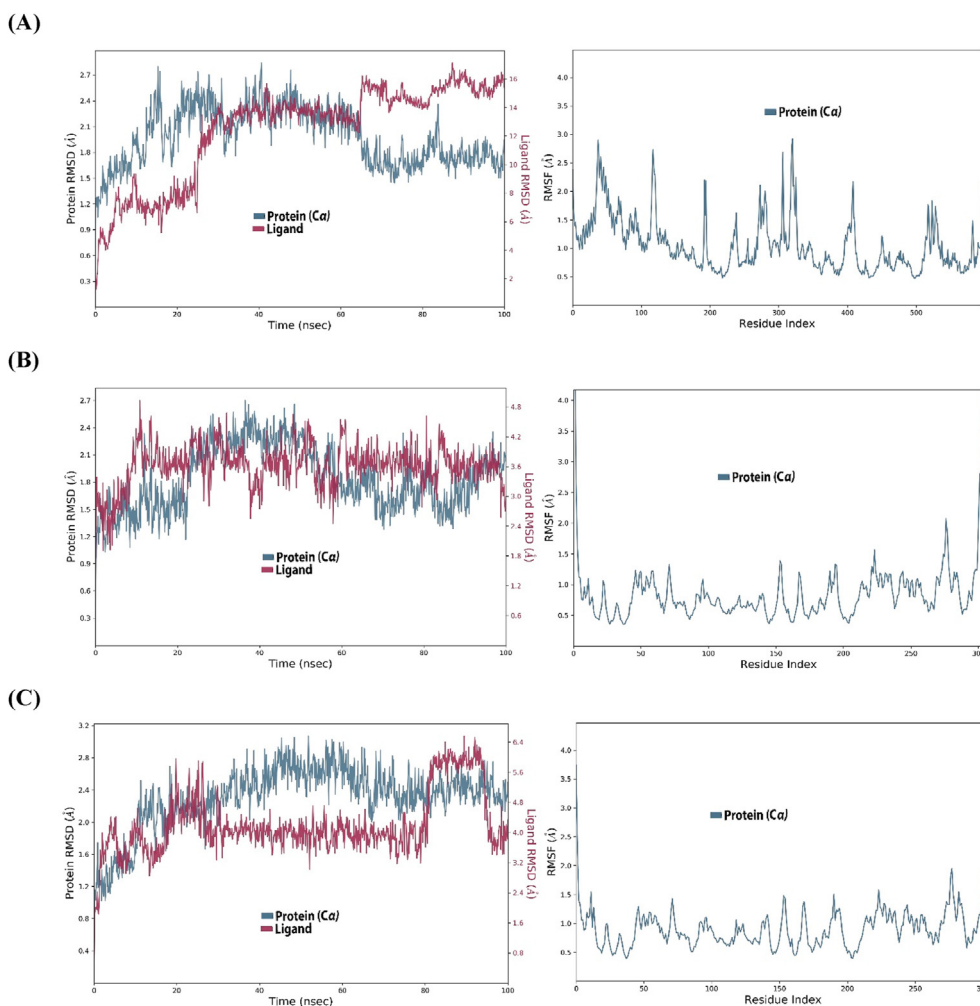


Figure 3. RMSD of the protein, RMSF of the protein amino acids, and RMSD of the docked poses of Telaprevir and N3 inside the protein binding sites during the simulation time of 100 ns for (A) Telaprevir (*hACE2*), (B) Telaprevir (M^{Pro}), and (C) N3 (M^{Pro}).

inhibitor inside its M^{Pro} binding pocket were Glu166, Gln189, Thr26, Gly143, and Asn142 during the simulation (75%–99%) (Figure 5C). Therefore, the higher number of contacts, especially for telaprevir within the M^{Pro} binding pocket, compared to its N3 inhibitor, reflects its superior stability and confirms the previously obtained higher docking score.

The ligand property study describes the ligand root mean square deviation (RMSD), radius of gyration (rGyr), molecular surface area (MolSA), solvent accessible surface area (SASA), and polar surface area (PSA). For the docked pose of telaprevir (*hACE2*), the RMSD was within the range of 2 Å. Its rGyr, which measures the extendedness of a ligand, was in the range of 4.8–6 Å and the equilibrium was approximately 5.4 Å. The MolSA, which is equivalent to a van der Waals surface area calculated with 1.4 Å probe radius, fluctuated from the start of the simulation until reaching equilibrium at 30 ns, and its range was observed between and 550–625 Å² with an equilibrium around 610 Å². Moreover, the surface area of telaprevir accessible by a water molecule (SASA) showed heavy fluctuations up to 20 ns, showed equilibrium between and 20–70 ns, and then fluctuated again until the end of the simulation time. The SASA range was approximately 150–600 Å², and the equilibrium was approximately 450 Å². Furthermore, the PSA, which refers to the SASA in telaprevir, contributed only to oxygen and nitrogen atoms. Its range was approximately 140–200 Å², and the equilibrium was approximately 160 Å² (Figure 6A). In contrast, regarding the docked pose of telaprevir (M^{Pro}), the RMSD was within the range of 1.75 Å. The rGyr was observed to be in the range of (4.75–5.50 Å) and the equilibrium was around 5.25 Å. It fluctuated only at the beginning until 10 ns and then

reached equilibrium until the end of the simulation time. The MolSA also fluctuated from the start of the simulation until reaching equilibrium at 10 ns, and its fluctuation range was between and 560–640 Å², with an equilibrium around 610 Å². Moreover, the SASA range was approximately 240–420 Å², and the equilibrium was approximately 330 Å². In addition, the PSA range was between 120 and 185 Å², and its equilibrium was approximately 160 Å² (Figure 6B). Collectively, the telaprevir property studied for its docked pose inside the M^{Pro} pocket were superior compared to its docked pose inside the *hACE2* pocket, which matches greatly with the previously discussed sections. Furthermore, for the docked pose of N3 (M^{Pro}), the RMSD was within the range of 3 Å. The rGyr was observed in the range of 5–7 Å, and the equilibrium was approximately 6 Å. The MolSA also fluctuated from the start of the simulation until it reached equilibrium at 10 ns and returned to fluctuations again at 80 ns. Its fluctuation range was between and 570–660 Å², with an equilibrium around 630 Å². Moreover, the SASA range was approximately 300–550 Å², and the equilibrium was approximately 350 Å². In addition, the PSA range was 200–275 Å², and its equilibrium was around 250 Å² (Figure 6C).

2.1.4. MD trajectory analysis and prime MM-GBSA calculations

The average MM-GBSA binding energy was calculated by applying the thermal_mmgbsa.py python script of Schrodinger, which also provides Coulomb, covalent binding, hydrogen-bonding, lipophilic, generalized Born electrostatic solvation, and van der Waals energies. All obtained values are listed in Table 4.

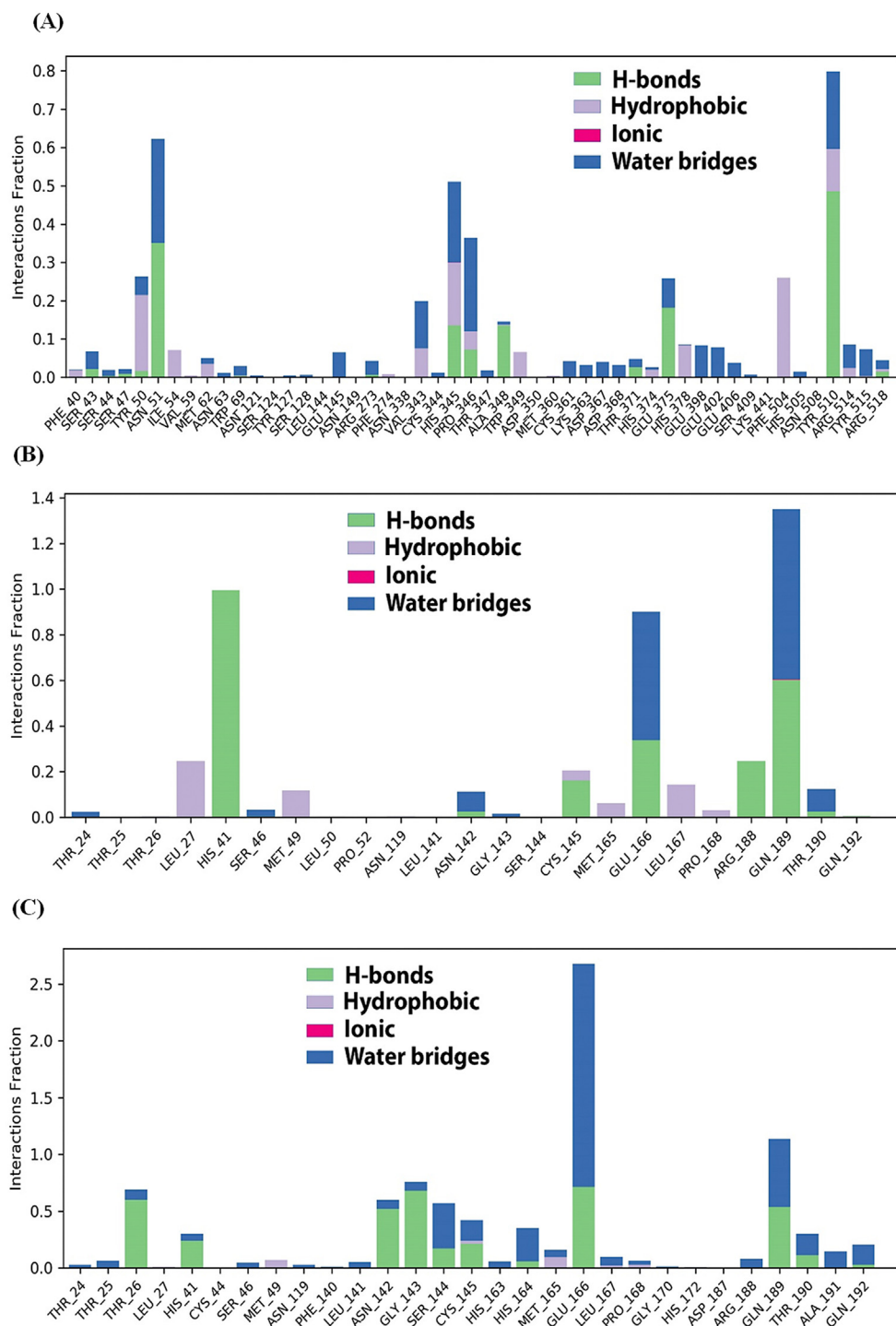


Figure 4. Protein-ligand contacts histograms for (A) Telaprevir (hACE2), (B) Telaprevir (MPro), and (C) N3 (MPro).

From the obtained MM-GBSA values, the binding energy for telaprevir inside the MPro receptor pocket was very promising compared to the co-crystallized N3 inhibitor with strong vdW interactions and lipophilic energy (Table 4).

2.1.5. In vitro validation

Based on our in silico studies, telaprevir showed the best evidence among the drugs to be selected for further in vitro validation against SARS-CoV-2. Telaprevir showed the best scores against direct (MPro) and

indirect (CTSL) viral targets. Hence, an in vitro study was conducted using telaprevir. To identify the appropriate concentrations to define the antiviral activity of telaprevir, the half-maximal cytotoxic concentration (CC50) was calculated using the crystal violet assay (Figure 7A), which was found to be 60.86.

Antiviral screening revealed that telaprevir exhibited promising cytotoxic inhibitory activity against NRC-03-nhCoV with IC50 = 11.55 μM (Figure 7B). Furthermore, it has promising antiviral activity with a high selectivity index (CC50/IC50 = 5.27).

3. Materials and methods

3.1. Selection of the studied drugs

A total of 16 DAAs, covering three DAA classes (eight NS3/4A, six NS5A, and two NS5B inhibitors) were collected from the literature and DrugBank [38, 39]. A list of the studied HCV DAAs is presented in Table 5.

3.2. In silico methods

3.2.1. Similarity ensemble approach (SEA)

This approach is a featured of in silico approach to assign new targets to ligands based on their chemical similarity [40]. Here, we used SEA to explore the targeting of studied DAAs to human targets that are important in SARS-CoV-2.

The DAA SMILES codes were retrieved from the Drug Bank 5.0 [39]. These files were fed to SEA in silico tools, including the SEA server (<http://sea.bkslab.org/>) [40], Swiss Target Prediction (<http://www.swisstargetprediction.ch/>) [41] and Poly pharmacology browser (<http://gdbtool.unibe.ch:8080/PPB/browser.html>) [42] to explore their off-label human targets that may suggest repurposing against SARS-CoV-2.

Gene (human targets) relevant scores for SARS-CoV-2 were retrieved from the GeneCards database (<https://www.GeneCards.org/>) [43]. The 10 best-relevant targets retrieved by GeneCards are shown in Table 6.

3.2.2. Docking studies

The 16 FDA-approved HCV DAA drugs were subjected to two separate molecular docking processes using MOE 2019.012 suite [44] against both the human angiotensin-converting enzyme 2 (hACE2) as an indirect target receptor and the main protease (M^{pro}) as a direct target receptor of SARS-CoV-2. This helps us examine their binding affinities and interactions with hACE2 and M^{pro} in order to propose the most appropriate mechanism of action and to prioritize the most promising members of the examined drugs. In addition, the co-crystallized native inhibitor (N3) of SARS-CoV-2 was docked and used as a reference standard in the docking process of viral M^{pro} .

3.2.2.1. Validation process. Before applying the docking processes using the Molecular Operating Environment (MOE) software package [45], a validation process was performed for the MOE program by subjecting the SARS-CoV-2 M^{pro} target to a separate redocking process for only its co-crystallized inhibitor (N3) inside its binding pocket, and a low RMSD value indicated a valid performance (RMSD = 1.43) [31].

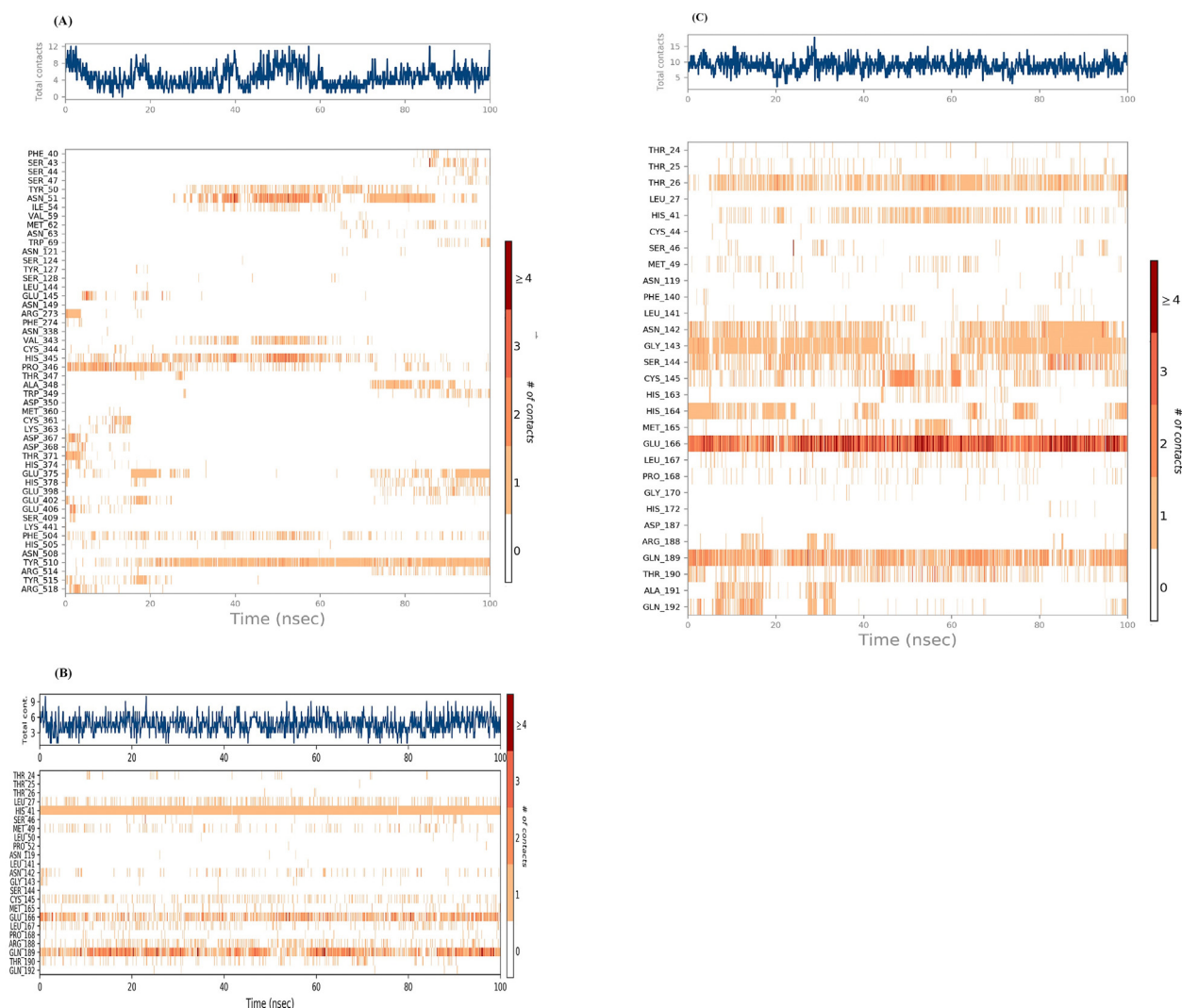


Figure 5. Heat map representing the number of protein–ligand contacts for (A) Telaprevir (hACE2), (B) Telaprevir (M^{pro}), and (C) N3 (M^{pro}).

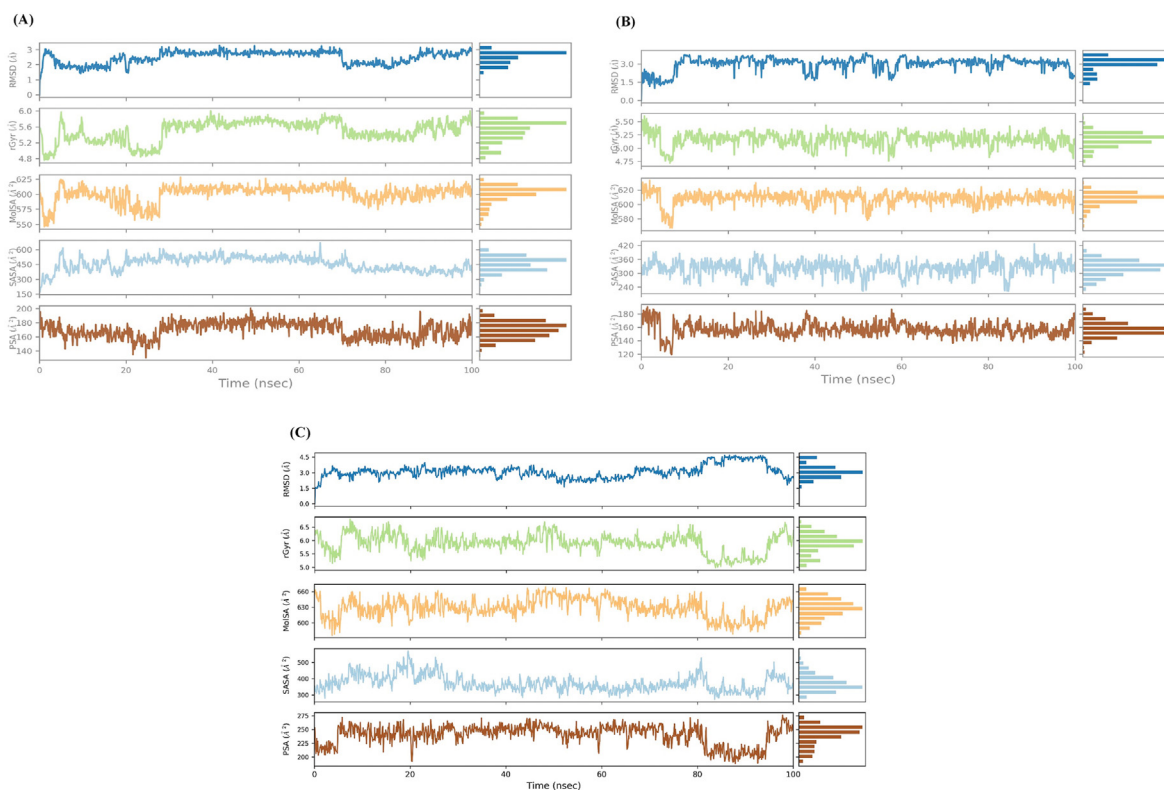


Figure 6. The ligand property trajectory of the (A) Telaprevir (*hACE2*), (B) Telaprevir (M^{pro}), and (C) N3 (M^{pro}) complexes during the 100 ns simulation time.

Table 4. Prime MM-GBSA energies for Telaprevir binding at both active sites of SARS-CoV-2 (*hACE2* and M^{pro}) and N3 inhibitor of M^{pro} .

Complex	ΔG Binding	Coulomb	Covalent	H-bond	Bind Packing	Lipo	Solv_GB	vdW	St. Dev.
Telaprevir (<i>hACE2</i>)	-47.87	-20.31	-1.81	-1.08	-9.30	-18.19	27.17	-48.61	4.67
Telaprevir (M^{pro})	-69.65	-23.41	-2.17	-1.22	-13.73	-19.85	32.77	-59.54	5.81
N3 (M^{pro})	-87.14	-25.00	-2.72	-1.36	-17.01	-21.14	37.98	-77.60	6.06

Coulomb: Coulomb energy; Covalent: Covalent binding energy; H-bond: Hydrogen-bonding energy; Lipo: Lipophilic energy; Solv_GB: Generalized Born electrostatic solvation energy; vdW: Van der Waals energy; St. Dev.: standard deviation.

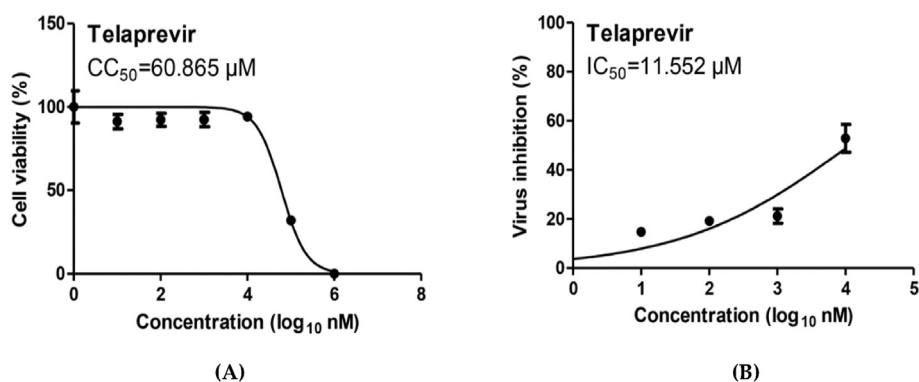


Figure 7. Dose-response and inhibition curves for Telaprevir. (a) Half maximal cytotoxic concentration (CC_{50}) in Vero E6 cells and (b) inhibitory concentration 50% (IC_{50}) against NRC-03-nhCoV were calculated using nonlinear regression analysis of GraphPad Prism.

3.2.2.2. Preparation of the sixteen FDA-approved HCV DAAs drugs. The chemical smiles of the examined FDA-approved HCV DAA drugs were copied from their respective pages in the PubChem website, inserted into the MOE builder, and then prepared for docking as previously discussed [46, 47]. The prepared drug members were inserted into two different databases for two separate docking processes against *hACE2* and M^{pro}

and saved as MDB files. The co-crystallized (N3) inhibitor was inserted into the database prepared for SARS-CoV-2 M^{pro} docking.

3.2.2.3. Preparation of *hACE2* and M^{pro} protein pockets of SARS-CoV-2. The X-ray structures of both *hACE2* and M^{pro} proteins (codes: 6VW1 [48] and 6LU7 [17], respectively) were extracted from the Protein Data Bank and

Table 5. The selected DAA drugs, their accession numbers, and their HCV targets collected from Drug Bank database.

No.	Drug	Target
1	Asunaprevir (DB11586)	NS3 protease inhibitor
2	Boceprevir (DB08873)	NS3/4A protease inhibitor
3	Glecaprevir (DB13879)	NS3/4A protease inhibitor
4	Grazoprevir (DB11575)	NS3/4A protease inhibitor
5	Paritaprevir (DB09297)	NS3/4A protease inhibitor
6	Simeprevir (DB06290)	NS3/4A protease inhibitor
7	Telaprevir (DB05521)	NS3/4A protease inhibitor
8	Voxilaprevir (DB12026)	NS3/4A protease inhibitor
9	Daclatasvir (DB09102)	NS5A inhibitor
10	Elbasvir (DB11574)	NS5A inhibitor
11	Ledipasvir (DB09027)	NS5A inhibitor
12	Ombitasvir (DB09296)	NS5A inhibitor
13	Pibrentasvir (DB13878)	NS5A inhibitor
14	Velpatasvir (DB11613)	NS5A inhibitor
15	Dasabuvir (DB09183)	NS5B polymerase inhibitor
16	Sofosbuvir (DB08934)	NS5B polymerase inhibitor

Table 6. The best ten relevant targets for SARS-CoV-2 as retrieved using Gene Cards database.

Gene	Description	Relevance score
ACE2	Angiotensin Converting Enzyme 2	59.95
TLR7	Toll Like Receptor 7	38.25
TMPS2	Transmembrane Serine Protease 2	30.49
NRP1	Neuropilin 1	23.36
FURIN	Furin, Paired Basic Amino Acid Cleaving Enzyme	18.65
DPP4	Dipeptidyl Peptidase 4	15.56
CTSL	Cathepsin L	15.47
HLA-A	Major Histocompatibility Complex, Class I, A	15.05
ACE	Angiotensin I Converting Enzyme	13.48
BSG	Basigin (Ok Blood Group)	13.04

each one was prepared for docking by applying the detailed procedure described earlier [49, 50].

3.2.2.4. Docking of the tested HCV drugs to the two binding pockets of SARS-CoV-2. Two separate docking processes against hACE2 and M^{Pro} pockets of SARS-CoV-2 were performed using the aforementioned databases. The docking methodology is described as follows: the prepared protein was opened in each docking process, and general docking was selected. The docking site for the hACE2 receptor was selected using dummy atoms to be the largest one, which contains a part of the receptor-binding domain (RBD) of SARS-CoV-2. However, the docking site in the case of M^{Pro} was the binding site of its co-crystallized native inhibitor N3. The placement methodology was specified as a triangle matcher, and the scoring methodology was selected as London dG. Moreover, the refinement methodology was applied as a rigid receptor, and the scoring methodology was GBVI/WSA, as described earlier [51, 52]. After completion of each docking process, the output poses were filtered, and the best one for each docked compound was selected for further investigation based on its score, RMSD-refine value, and binding interactions.

3.2.3. Molecular dynamics (MD) simulations

MD simulations were performed using the Desmond module of the Schrödinger LLC package [53]. Each simulation was run for 100 ns, and the relaxation time for all the selected poses was 1 ps. The applied simulation system was kept inside an orthorhombic box 10 Å away from the tested protein to retain the periodic boundary states. The box was filled with water, as described using the TIP3P model [54]. Moreover, the

protein and ligand parameters were measured by applying the OPLS3 force field [55], and the Desmond system builder was used to adjust the salt concentration at 0.15 M NaCl [56]. MD simulations were applied to the NPT ensemble (constant number of particles, pressure, and temperature). The pressure and temperature were kept constant at 1 atm and 300 K using the Martyna–Tuckerman–Klein chain coupling and Nosé–Hoover chain coupling schemes, respectively [57, 58]. A cut-off radius of 0.9 Å was used to calculate the Coulombic interactions.

3.2.4. MD trajectory analysis and prime MM-GBSA calculations

Maestro software was used to evaluate the effect of interactions on the stability of the ligand-protein complexes. The MM-GBSA was performed to study both the ligand strain and binding energies for the docked poses throughout the 100 ns period of the MD simulation using the thermal_mmgbsa.py python script of Schrodinger.

3.3. In vitro methods

3.3.1. Cytotoxicity (CC₅₀) determination

Telaprevir was obtained from Sigma-Aldrich and dissolved in dimethyl sulfoxide (DMSO, Sigma-Aldrich) at a concentration of 100 mM and stored at 4 °C. To assess the CC₅₀, the stock solution of telaprevir was diluted further to the working solutions with DMEM (1000 µM–0.01 µM). Cytotoxic activity was tested in VERO-E6 cells using a crystal violet assay as previously described [59] with minor modifications. Briefly, the cells were seeded in 96-well plates (100 µL/well at a density of 3 × 10⁵ cells/ml) and incubated for 24 h at 37 °C in 5% CO₂. After 24 h, the cells were treated with various concentrations of telaprevir in triplicate. At 72 h post-treatment, the supernatant was discarded, and cell monolayers were fixed with 10% formaldehyde for 1 h at room temperature (RT). The fixed monolayers were then dried thoroughly and stained with 50 µL of 0.1% crystal violet for 20 min on a bench rocker at room temperature. The monolayers were then washed, dried overnight, and the crystal violet dye in each well was dissolved in 200 µL methanol for 20 min on a bench rocker at room temperature. The absorbance of the crystal violet solutions was measured at λ_{max} 570 nm as a reference wavelength using a multi-well plate reader. The CC₅₀ value was calculated using nonlinear regression analysis using GraphPad Prism software (version 5.01) by plotting log concentrations of telaprevir versus normalized response (variable slope).

3.3.2. Inhibitory concentration 50 (IC₅₀) determination

The IC₅₀ values for telaprevir were determined as previously described [12], with minor modifications. Briefly, in 96-well tissue culture plates, 2.4 × 10⁴ Vero-E6 cells were distributed in each well and incubated overnight at 37 °C in a humidified incubator with 5% CO₂. The cell monolayers were washed once with 1x PBS. An aliquot of the SARS-CoV-2 “NRC-03-nhCoV” virus [60] containing 100 TCID₅₀ was incubated with serial diluted concentrations of the tested compound and kept at 37 °C for 1 h. The Vero-E6 cell monolayers were treated with virus/compound mixtures and incubated at 37 °C in a total volume of 200 µL per well. Untreated cells that are infected with the virus to represent “virus control,” with cells that are not treated and not infected being the “cell control” Following incubation at 37 °C in a 5% CO₂ incubator for 72 h, the cells were fixed with 100 µl of 10% paraformaldehyde for 20 min and stained with 0.5% crystal violet in distilled water for 15 min at RT. The crystal violet dye was then dissolved using 100 µl absolute methanol per well, and the optical density of the color was measured at 570 nm using 200rt plate reader (Anthos Labtec Instruments, Heerhugowaard, Netherlands). The inhibitory concentration 50% (IC₅₀) of the compound is required to reduce the virus-induced cytopathic effect (CPE) by 50% relative to the virus control. The IC₅₀ value was calculated using nonlinear regression analysis using GraphPad Prism software (version 5.01) by plotting log concentrations of telaprevir versus the normalized response (variable slope).

4. Conclusion

Drug repurposing is a marvelous strategy that helps in rapid response to pandemics. As antivirals showed a great ability to be repurposed against different viruses, we selected a group of 16 HCV DAAs to study their potential for repurposing against SARS-CoV-2. Among the studied drugs, telaprevir showed the best *in silico* evidence for its repurposing potential against SARS-CoV-2. Molecular docking results revealed the superior ability of telaprevir to fit with the M^{pro} pocket of SARS-CoV-2 through the formation of three H-bonds with the key protein residues. Additionally, molecular dynamics studies of the docked pose of telaprevir inside the M^{pro} pocket revealed its greater stability compared to that inside the hACE2 pocket, which confirmed the previously obtained docking results. Furthermore, the MM-GBSA binding energy showed that telaprevir docked pose inside the M^{pro} pocket had very promising binding energy compared to that of the N3 inhibitor. *In vitro* studies have inferred this potential (IC₅₀ = 11.55 μM, CC₅₀ = 60.865 μM, and CC₅₀/IC₅₀ = 5.27), and we recommend further preclinical and clinical studies for the ability of telaprevir to be successfully repurposed against SARS-CoV-2. Although different publications were published on SARS-CoV-2, to our knowledge, this is the first study to focus on telaprevir as a promising drug member to be repurposed towards SARS-CoV-2 using both computational and *in vitro* confirmatory aspects.

Declarations

Author contribution statement

Amal Mahmoud: Conceived and designed the experiments; Analyzed and interpreted the data; Wrote the paper.

Ahmed Mostafa: Conceived and designed the experiments; Performed the experiments; Analyzed and interpreted the data; Contributed reagents, materials, analysis tools or data; Wrote the paper.

Ahmed A. Al-Karmalawy: Performed the experiments; Analyzed and interpreted the data; Contributed reagents, materials, analysis tools or data; Wrote the paper.

Ahmad Zidan, Hamada S. Abulkhair, Sara H. Mahmoud, Mahmoud Shehata: Performed the experiments; Wrote the paper.

Mahmoud M. Elhefnawi: Analyzed and interpreted the data; Wrote the paper.

Mohamed A. Ali: Conceived and designed the experiments; Analyzed and interpreted the data; Contributed reagents, materials, analysis tools or data; Wrote the paper.

Funding statement

This work was supported by the Deanship of Scientific Research, Imam Abdulrahman Bin Faisal University, Dammam, Saudi Arabia, Grant No. Covid 19-2020-001-BASRC. This research was also funded in part by the Egyptian National Research Centre (NRC) under contract number MP120801 and by the Egyptian Academy of Scientific Research & Technology (ASRT) within the "Ideation Fund" program under contract number 7303. This research was funded by the National Institute of Allergy and Infectious Diseases, National Institutes of Health (under contract HHSN272201400006C).

Data availability statement

Data will be made available on request.

Competing interest statement

The authors declare no conflict of interest.

Additional information

Supplementary content related to this article has been published online at <https://doi.org/10.1016/j.heliyon.2021.e07962>.

References

- [1] Y. Wang, et al., Remdesivir in adults with severe COVID-19: a randomised, double-blind, placebo-controlled, multicentre trial, *Lancet* 395 (10236) (2020) 1569–1578.
- [2] A. Mostafa, et al., Middle East respiratory syndrome coronavirus (MERS-CoV): state of the science, *Microorganisms* 8 (7) (2020).
- [3] P. V'kovski, et al., Coronavirus biology and replication: implications for SARS-CoV-2, *Nat. Rev. Microbiol.* 19 (3) (2021) 155–170.
- [4] D. Schmiede, et al., One Health in the context of coronavirus outbreaks: a systematic literature review, *One Health* 10 (2020) 100170.
- [5] A.A. Sarhan, N.A. Ashour, A.A. Al-Karmalawy, The journey of antimalarial drugs against SARS-CoV-2: review article, *Informat. Med. Unlocked* (2021) 100604.
- [6] D.B. Mahmoud, Z. Shitu, A. Mostafa, Drug repurposing of nitazoxanide: can it be an effective therapy for COVID-19? *J. Genet. Engin. Biotechnol.* 18 (1) (2020) 35, 35.
- [7] C. Harrison, Coronavirus puts drug repurposing on the fast track, *Nat. Biotechnol.* 38 (4) (2020) 379–381.
- [8] A.A. Zaki, et al., Calendulaglycoside A showing potential activity against SARS-CoV-2 main protease: molecular docking, molecular dynamics, and SAR studies, *J. Tradit. Complem. Med.* (2021).
- [9] A.A. Elmaaty, et al., In a search for potential drug candidates for combating COVID-19: computational study revealed salvianolic acid B as a potential therapeutic targeting 3CLpro and spike proteins, *J. Biomol. Struct. Dyn.* (2021) 1–28.
- [10] A. Kandeil, et al., Bioactive polyphenolic compounds showing strong antiviral activities against severe acute respiratory syndrome coronavirus 2, *Pathogens* 10 (6) (2021) 758.
- [11] R. Soltane, et al., Strong inhibitory activity and action modes of synthetic maslinic acid derivative on highly pathogenic coronaviruses: COVID-19 drug candidate, *Pathogens* 10 (5) (2021) 623.
- [12] A. Mostafa, et al., FDA-approved drugs with potent *in vitro* antiviral activity against severe acute respiratory syndrome coronavirus 2, *Pharmaceuticals* 13 (12) (2020) 443.
- [13] A.A. Al-Karmalawy, I.H.J.P.S. Eissa, Molecular Docking and Dynamics Simulations Reveal the Potential of Anti-HCV Drugs to Inhibit COVID-19 Main Protease, 2021.
- [14] B. Mercorelli, G. Palu, A. Lorigian, Drug repurposing for viral infectious diseases: how far are we? *Trends Microbiol.* 26 (10) (2018) 865–876.
- [15] T. Pietschmann, Clinically approved ion channel inhibitors close gates for hepatitis C virus and open doors for drug repurposing in infectious viral diseases, *J. Virol.* 91 (2) (2017).
- [16] S.A. Amin, et al., First structure-activity relationship analysis of SARS-CoV-2 virus main protease (Mpro) inhibitors: an endeavor on COVID-19 drug discovery, *Mol. Divers.* (2021).
- [17] Z. Jin, et al., Structure of M(pro) from SARS-CoV-2 and discovery of its inhibitors, *Nature* 582 (7811) (2020) 289–293.
- [18] G. Simmons, et al., Inhibitors of cathepsin L prevent severe acute respiratory syndrome coronavirus entry, *Proc. Natl. Acad. Sci. U. S. A.* 102 (33) (2005) 11876–11881.
- [19] H.P. Jia, et al., ACE2 receptor expression and severe acute respiratory syndrome coronavirus infection depend on differentiation of human airway epithelia, *J. Virol.* 79 (23) (2005) 14614–14621.
- [20] A.K. Padhi, T. Tripathi, Targeted design of drug binding sites in the main protease of SARS-CoV-2 reveals potential signatures of adaptation, *Biochem. Biophys. Res. Commun.* 555 (2021) 147–153.
- [21] M. Liu, et al., Potential role of ACE2 in coronavirus disease 2019 (COVID-19) prevention and management, *J. Transl. Int. Med.* 8 (1) (2020) 9–19.
- [22] A.A. Al-Karmalawy, et al., Molecular docking and dynamics simulation revealed the potential inhibitory activity of ACEIs against SARS-CoV-2 targeting the hACE2 receptor, *Front. Chem.* 9 (227) (2021).
- [23] T. Liu, et al., Cathepsin L-selective inhibitors: a potentially promising treatment for COVID-19 patients, *Pharmacol. Ther.* 213 (2020) 107587.
- [24] A.K. Padhi, T. Tripathi, Can SARS-CoV-2 accumulate mutations in the S-protein to increase pathogenicity? *ACS Pharmacol Transl Sci* 3 (5) (2020) 1023–1026.
- [25] C. Isgrò, A.M. Sardanelli, L.L. Palese, Systematic search for SARS-CoV-2 main protease inhibitors for drug repurposing: ethacrynic acid as a potential drug, *Viruses* 13 (1) (2021).
- [26] L. Fu, et al., Both Boceprevir and GC376 efficaciously inhibit SARS-CoV-2 by targeting its main protease, *Nat. Commun.* 11 (1) (2020) 4417.
- [27] A.K. Padhi, et al., High-throughput rational design of the remdesivir binding site in the RdRp of SARS-CoV-2: implications for potential resistance, *iScience* 24 (1) (2021) 101992.
- [28] A. Abo Elmaaty, et al., Computational insights on the potential of some NSAIDs for treating COVID-19: priority set and lead optimization, *Molecules* 26 (12) (2021) 3772.
- [29] A.A. Elmaaty, et al., Revisiting activity of some glucocorticoids as a potential inhibitor of SARS-CoV-2 main protease: theoretical study, *RSC Adv.* 11 (17) (2021) 10027–10042.
- [30] N.J. Liverton, et al., MK-7009, a potent and selective inhibitor of hepatitis C virus NS3/4A protease, *Antimicrob. Agents Chemother.* 54 (1) (2010) 305–311.
- [31] B.J. McConkey, V. Sobolev, M. Edelman, The performance of current methods in ligand–protein docking, *Curr. Sci.* (2002) 845–856.

- [32] S.G. Eliaa, et al., Empagliflozin and doxorubicin synergistically inhibit the survival of triple-negative breast cancer cells via interfering with the mTOR pathway and inhibition of calmodulin: in vitro and molecular docking studies, *ACS Pharmacol. Translat. Sci.* 3 (6) (2020) 1330–1338.
- [33] K.V. Miroshnychenko, A.V. Shestopalova, Combined use of the hepatitis C drugs and amentoflavone could interfere with binding of the spike glycoprotein of SARS-CoV-2 to ACE2: the results of a molecular simulation study, *J. Biomol. Struct. Dyn.* (2021) 1–15.
- [34] K. Bafna, R.M. Krug, G.T. Montelione, Structural similarity of SARS-CoV2 M(pro) and HCV NS3/4A proteases suggests new approaches for identifying existing drugs useful as COVID-19 therapeutics, *ChemRxiv* (2020).
- [35] K. Bafna, et al., Hepatitis C virus drugs that inhibit SARS-CoV-2 papain-like protease synergize with remdesivir to suppress viral replication in cell culture, *Cell Rep.* 35 (7) (2021) 109133.
- [36] D.W. Kneller, et al., Malleability of the SARS-CoV-2 3CL M(pro) active-site cavity facilitates binding of clinical antivirals, *Structure* 28 (12) (2020) 1313–1320 e3.
- [37] A.K. Padhi, S.L. Rath, T. Tripathi, Accelerating COVID-19 research using molecular dynamics simulation, *J. Phys. Chem. B* (2021).
- [38] A. Geddawy, et al., Direct acting anti-hepatitis C virus drugs: clinical pharmacology and future direction, *J. Transl. Int. Med.* 5 (1) (2017) 8–17.
- [39] D.S. Wishart, et al., DrugBank 5.0: a major update to the DrugBank database for 2018, *Nucleic Acids Res.* 46 (D1) (2018) D1074–D1082.
- [40] M.J. Keiser, et al., Relating protein pharmacology by ligand chemistry, *Nat. Biotechnol.* 25 (2) (2007) 197–206.
- [41] D. Gfeller, et al., SwissTargetPrediction: a web server for target prediction of bioactive small molecules, *Nucleic Acids Res.* 42 (Web Server issue) (2014) W32–W38.
- [42] M. Awale, J.-L. Reymond, The polypharmacology browser: a web-based multi-fingerprint target prediction tool using ChEMBL bioactivity data, *J. Cheminf.* 9 (1) (2017) 11.
- [43] G. Stelzer, et al., The GeneCards suite: from gene data mining to disease genome sequence analyses, *Curr. Protoc. Bioinform.* 54 (2016), 1 30 1-1 30 33.
- [44] S. Vilar, G. Cozza, S. Moro, Medicinal chemistry and the molecular operating environment (MOE): application of QSAR and molecular docking to drug discovery, *Curr. Top. Med. Chem.* 8 (18) (2008) 1555–1572.
- [45] Inc., C.C.G., Molecular Operating Environment (MOE), 2016. Chemical Computing Group Inc 1010 Sherbooke St. West, Suite# 910, Montreal.
- [46] A. Ghanem, et al., Tanshinone IIA synergistically enhances the antitumor activity of doxorubicin by interfering with the PI3K/AKT/mTOR pathway and inhibition of topoisomerase II: in vitro and molecular docking studies, *New J. Chem.* 44 (40) (2020) 17374–17381.
- [47] M. Khattab, A.A. Al-Karmalawy, Revisiting activity of some nocodazole analogues as a potential anticancer drugs using molecular docking and DFT calculations, *Front. Chem.* 9 (92) (2021).
- [48] J. Shang, et al., Structural basis of receptor recognition by SARS-CoV-2, *Nature* 581 (7807) (2020) 221–224.
- [49] R.M. Samra, et al., Bioassay-guided isolation of a new cytotoxic ceramide from *Cyperus rotundus* L, *South Afr. J. Bot.* 139 (2021) 210–216.
- [50] A.A. Al-Karmalawy, M. Khattab, Molecular modelling of mebendazole polymorphs as a potential colchicine binding site inhibitor, *New J. Chem.* 44 (33) (2020) 13990–13996.
- [51] A.A. Zaki, et al., Molecular docking reveals the potential of *Cleome amblyocarpa* isolated compounds to inhibit COVID-19 virus main protease, *New J. Chem.* 44 (39) (2020) 16752–16758.
- [52] R. Alnajjar, et al., Molecular docking, molecular dynamics, and in vitro studies reveal the potential of angiotensin II receptor blockers to inhibit the COVID-19 main protease, *Heliyon* 6 (12) (2020), e05641.
- [53] S. Release, 3: Desmond Molecular Dynamics System, DE Shaw Research, New York, NY, Maestro-Desmond Interoperability Tools, Schrödinger, New York, NY, 2017, 2017.
- [54] W.L. Jorgensen, et al., Comparison of simple potential functions for simulating liquid water, *J. Chem. Phys.* 79 (2) (1983) 926–935.
- [55] E. Harder, et al., OPLS3: a force field providing broad coverage of drug-like small molecules and proteins, *J. Chem. Theor. Comput.* 12 (1) (2016) 281–296.
- [56] M. Bergdorf, et al., Desmond/GPU Performance as of October 2015, DE Shaw research, 2015.
- [57] G.J. Martyna, M.L. Klein, M. Tuckerman, Nosé–Hoover chains: the canonical ensemble via continuous dynamics, *J. Chem. Phys.* 97 (4) (1992) 2635–2643.
- [58] G.J. Martyna, D.J. Tobias, M.L. Klein, Constant pressure molecular dynamics algorithms, *J. Chem. Phys.* 101 (5) (1994) 4177–4189.
- [59] M. Feoktistova, P. Geserick, M. Leverkus, Crystal violet assay for determining viability of cultured cells, *Cold Spring Harb. Protoc.* 2016 (4) (2016), prot087379.
- [60] A. Kandeil, et al., Coding-complete genome sequences of two SARS-CoV-2 isolates from Egypt, *Microbiol. Res. Announc.* 9 (22) (2020) e00489–e00520.